

Supplementary Information

Revealing the critical pore size for hydrogen storage via simultaneous enclathration and physisorption in activated carbon

Erling Velten Rothmund*, Jianying He, Zhiliang Zhang, and Senbo Xiao*

¹Department of Structural Engineering, Norwegian University of Science and Technology (NTNU),
Trondheim 7491, Norway

*E-mail: erling.v.rothmund@ntnu.no, senbo.xiao@ntnu.no

1 Equilibration of molecular dynamics trajectories

1.1 Model verification simulations

The main manuscript performs verification of an empirical model by comparing equivalent simulations of hydrogen hydrate conducted with force field molecular dynamics (FFMD) using GROMACS¹ and ab-initio molecular dynamics (AIMD) using VASP²⁻⁵. To check convergence and stability in both methods, the time evolution of potential energy, temperature, pressure, and lattice parameters for the S1L4 cage configuration is shown in Fig. 1. The absence of visible trends in any of the plots indicates sufficient equilibration of the initial configuration in both systems. Stability over time in energy, temperature, pressure, and lattice vectors (volume) indicates stable and reliable simulations. The mean values of temperature and pressure are consistent between AIMD and FFMD, with slight variations in energy and lattice parameters being explored in section 3.1 of the main manuscript. Therefore, these trajectories are suitable for sampling thermodynamic properties in the equilibrium system.

From the plots of Fig. 1, it is apparent that fluctuations of various properties are larger in AIMD than in FFMD. However, direct comparison is not appropriate because the FFMD simulation cell is 8 times larger than in AIMD. Intuitively, larger systems exhibit smaller fluctuations due to properties being averaged over more particles, and random fluctuations in different regions partly cancelling each other out. A precise relation follows from the statistical arguments in §2 of Landau & Lifshitz classical textbook⁶, stating that the relative root-mean-square fluctuations of a thermodynamic property f behaves as:

$$\frac{\sqrt{\langle \Delta f^2 \rangle}}{\langle f \rangle} \propto 1/\sqrt{N} \propto 1/\sqrt{V}, \quad (1)$$

where N is the number of particles in the system with volume V . Further derivations in §114

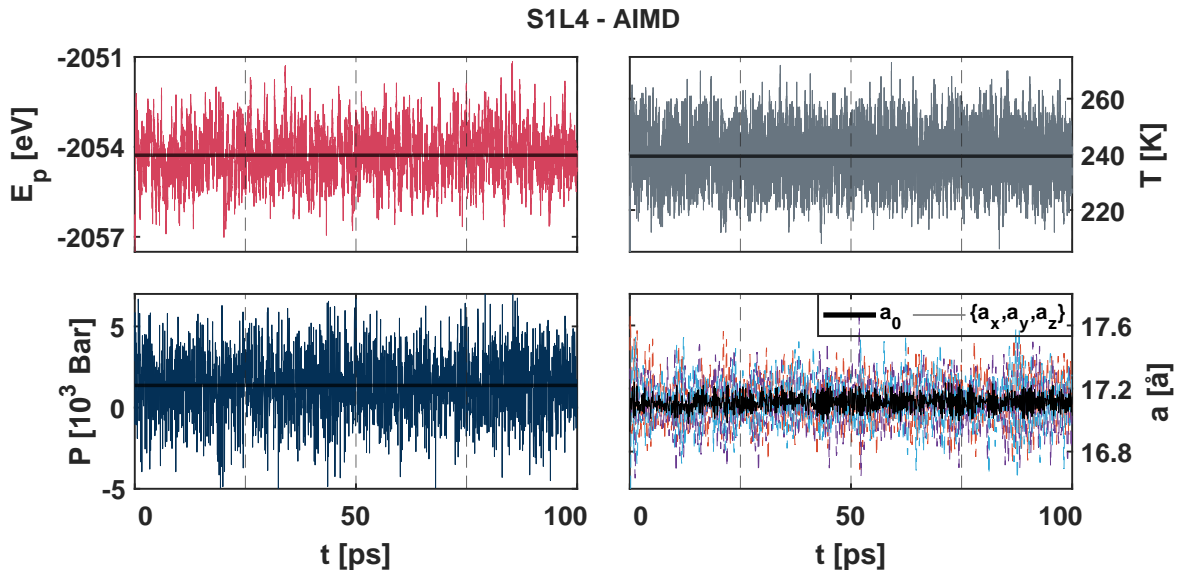
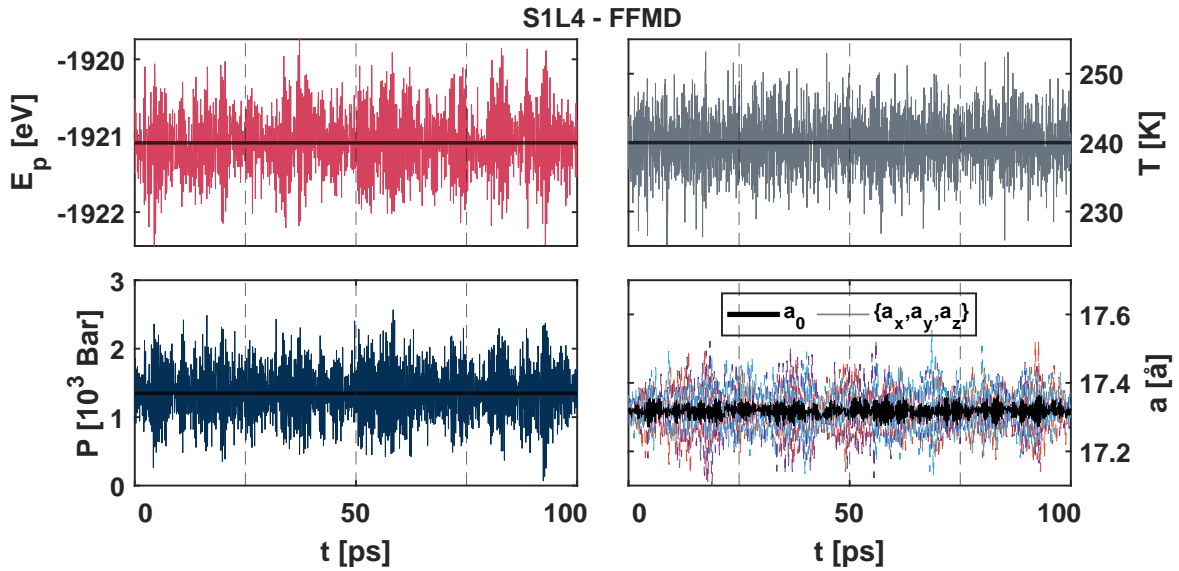


Figure 1: System equilibration check for (a) FFMD and (b) AIMD simulations of the S1L4 hydrogen hydrate configuration. Equivalent equilibration trajectory checks were performed for every configuration. The absence of trends or instabilities indicates reliable equilibrium sampling.

provide the more specific relationships for volume, pressure P , and temperature T :

$$\begin{aligned}\frac{\sqrt{\langle \Delta V^2 \rangle}}{\langle V \rangle} &\propto 1/\sqrt{V} \\ \sqrt{\langle \Delta P^2 \rangle} &\propto 1/\sqrt{V} \\ \sqrt{\langle \Delta T^2 \rangle} &\propto 1/\sqrt{V}.\end{aligned}\tag{2}$$

Applying the standard propagation of uncertainty formula for estimating the fluctuations in unit-cell lattice parameter, assuming a cubic unit cell ($V = a_0^3$), and introducing shorthand notation $\sigma(f) = \sqrt{\langle \Delta f^2 \rangle}$ yields:

$$\begin{aligned}\sigma(V) &= \sqrt{\left(\frac{\partial V}{\partial a_0}\right)^2 \sigma(a_0)^2} = \sqrt{(3a_0^2)^2 \sigma(a_0)^2} = 3a_0^2 \sigma(a_0) \\ \frac{\sigma(V)}{\langle V \rangle} &= \frac{3a_0^2 \sigma(a_0)}{\langle a_0^3 \rangle} \propto \frac{\sigma(a_0)}{\langle a_0 \rangle} \\ \implies \frac{\sigma(a_0)}{\langle a_0 \rangle} &\propto 1/\sqrt{V},\end{aligned}\tag{3}$$

where the last implication comes from Eqn. 2. Eqn. 3 states that fluctuations in the lattice parameter relative to average lattice parameter behaves the same as fluctuations in volume relative to average system volume. Consequently, a system with 8 unit cells will have total volume fluctuations that are $\sqrt{8}$ times larger than the equivalent system with 1 unit cell. However, when calculating *relative* volume or relative lattice parameter fluctuations for 1 unit cell of the 8 unit cell system ($V/8$ or $a_0 \sim (V/8)^{1/3}$), the resulting values will have root-mean-square fluctuations that are *smaller* by a factor $1/\sqrt{8}$.

The above discussion on thermodynamic fluctuations largely explains the differences observed between FFMD and AIMD. The theory suggests that all properties displayed in Fig. 1 should exhibit fluctuations $\sqrt{8}$ larger in AIMD than FFMD. Indeed, the observed fluctuations in lattice parameter a_0 are equivalent between AIMD and FFMD after accounting for the difference in simulation cell volume, indicating consistent lattice behaviour between the two methods. Note that in Figure 7 of the main article, the FFMD fluctuations of a_0 were increased by a factor

$\sqrt{8}$ to correspond to the AIMD system.

However, temperature and pressure fluctuations show some inconsistency. Temperature fluctuations are 0.74 times smaller and pressure fluctuations 1.87 times larger in AIMD than FFMD after volume correction. This discrepancy may stem from the use of different temperature-coupling algorithms, variations in the pressure-coupling algorithm implementations, and differences in how pressure is defined and calculated between the two MD engines. It may also result from FFMD's inaccuracies in pressure estimation due to the Lennard-Jones potential poorly approximating repulsive forces. Considering that the more physically significant lattice vectors behave consistently, the inconsistency in pressure fluctuations can be regarded as a technical artifact of the simulation algorithms.

1.2 Equilibration of hydrogen hydrate in activated carbon simulations

The MD simulations in this work aim to study the equilibrium structure of hydrogen hydrate in activated carbon after partial decomposition. Therefore, an equilibration check similar to the previous section was performed for each hydrogen hydrate in activated carbon simulation system. The analysis of the 5 repetitions of one representative system (with "default" parameters $T = 220$, $P = 1350$ bar, $\rho = 0.35$ g/cm³, $S_{\text{fragment}} = 150$, $R_{\text{defect}} = 0.1$, and $R_{\text{OH}} = 0.38$) considering potential energy, temperature, pressure, volume, and total hydrate quantity is shown in Fig. 2. The trajectories exhibit stable energy, temperature, and pressure, with expected fluctuations. The gradual increase in volume is likely due to gas molecules escaping from hydrate cages and forming less-dense gas bubbles in the micropores of activated carbon, and the subsequent structural readjustment of the individual fullerene fragments. This behaviour plateaus, though it is unclear if equilibrium is fully achieved in all simulations. Notably, the volume was fully stable in simulations at a higher pressure ($P = 2700$ bar). Slow gas migration might be avoided if the simulation system, like its real-world counterpart, was under a high gas pressure constantly resupplying H₂, or if the activated carbon micropores were initially saturated with H₂. Nevertheless, the energy and total hydrate quantity plateau more clearly, indicating that the hydrate structure within the porous host is stable. Consequently, the final 10ns of the simulation trajectories seem sufficiently well equilibrated for extracting results, such as the critical pore size or qualitatively accurate distribution of hydrogen gas molecules.

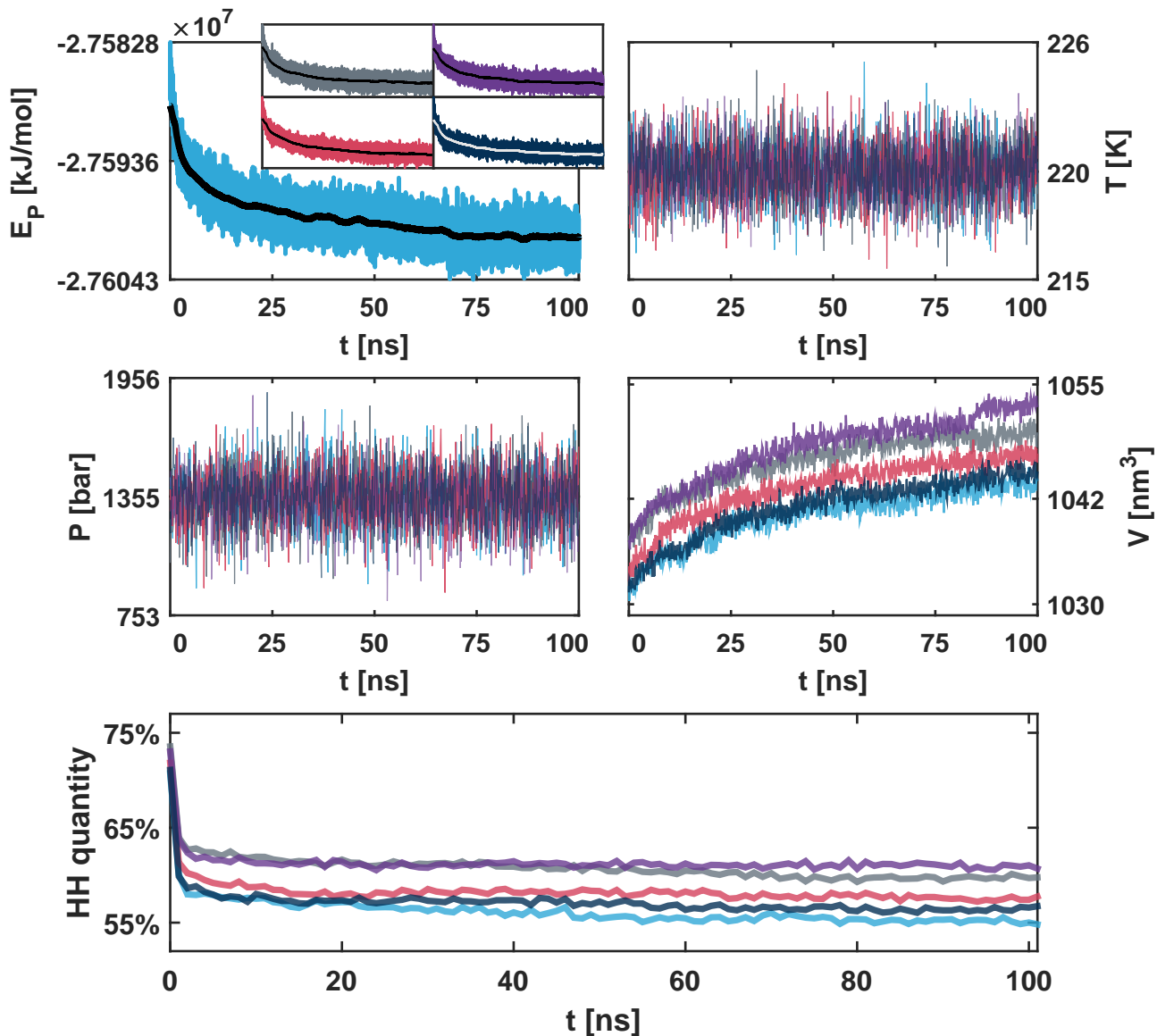


Figure 2: Equilibrium check for simulation trajectories of hydrogen hydrate in activated carbon. The system state is monitored by the potential energy E_P , temperature T , pressure P , volume V , and total hydrate quantity as a fraction of water molecules in the hydrate phase throughout the simulation trajectory. Each coloured line represents one of the first five repetitions of simulations with different randomized structures using the "default" set of parameters. Equivalent checks were performed for all simulations.

2 Using VASP on-the-fly machine learning to accelerate ab-initio molecular dynamics

Ab-initio molecular dynamics (AIMD) simulations using VASP were performed to assess the accuracy of force-field molecular dynamics (FFMD) in simulating hydrogen hydrate by performing equivalent simulations with the two methods. However, to accelerate the AIMD simulations and capture important dynamics such as H₂ motion through hydrate cages, AIMD simulations with on-the-fly machine learning (ML-AIMD)⁷⁻⁹ was employed. This section aims to establish confidence in the ML-AIMD approach for this specific use case by comparing its simulations directly with simulations from pure AIMD.

On-the-fly ML-AIMD simulations begin identically to normal AIMD simulations. During each step of DFT calculations in the AIMD procedure, a machine learning force-field is trained to replicate the forces (output) based on atomic positions (input). After a sufficient accumulation of DFT calculations, VASP determines that the ML force-field produces outputs adequately close to DFT results, allowing it to take over and perform vastly faster MD steps using the trained ML force-field. As the simulation system gradually changes due to atomic motion, VASP performs more DFT calculations to update the ML force-field. In theory, with a strict enough algorithm for choosing between DFT and ML steps, ML-AIMD should yield equivalent results to AIMD, but with a significant speedup. ML-AIMD was run exclusively in "training mode", starting the ML force-field from scratch each time. Default settings for ML-AIMD provided by VASP were used (except for "ML_CX=-0.1" which biases the software towards performing more DFT and fewer ML calculations). On-the-fly ML is generally less prone to catastrophic failure than pre-trained potentials, which heavily depend on the quality of its training data, albeit with a performance tradeoff.

ML-AIMD was found to closely reproduce the results of AIMD by conducting equivalent

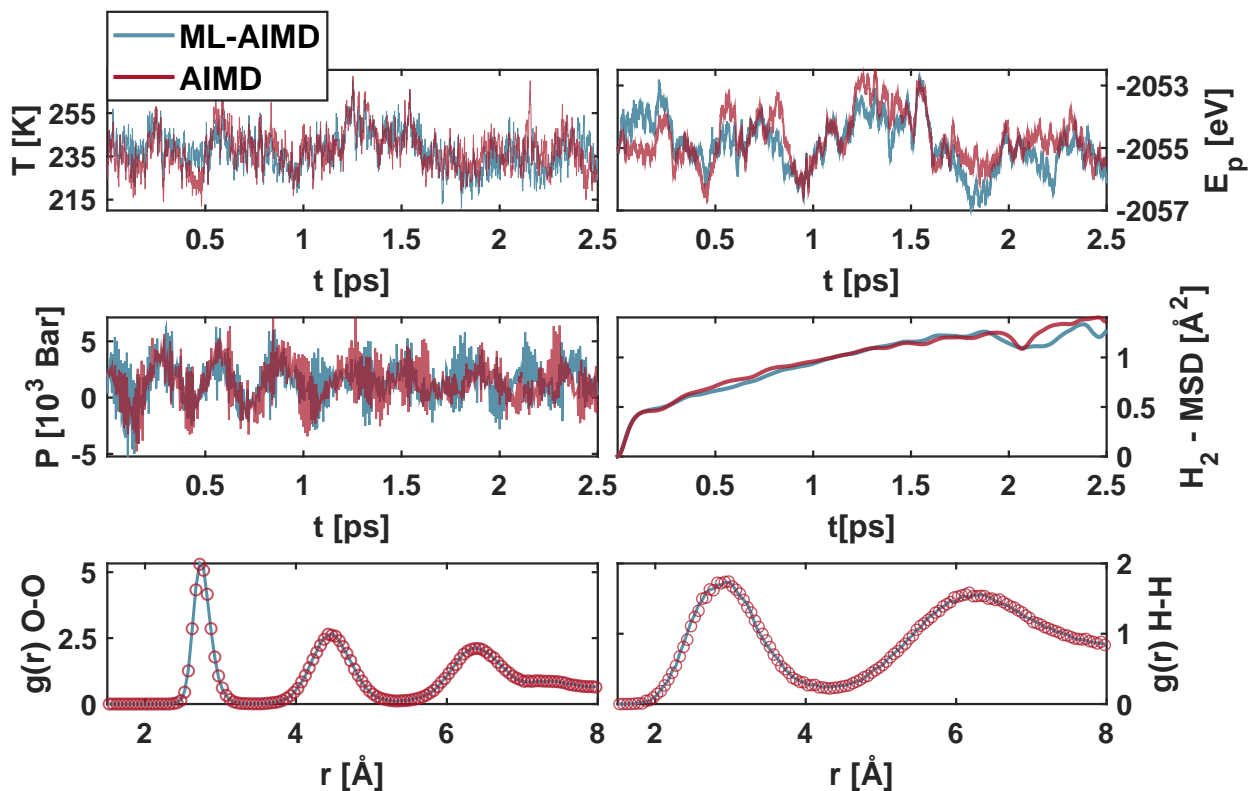


Figure 3: Comparison between normal AIMD (red) and ML-AIMD (blue). From left to to right, top to bottom, the first 4 panels show temperature, potential energy, pressure, and H_2 MSD during the simulation trajectories. The last two panels show oxygen-oxygen and hydrogen-hydrogen radial distribution functions (for H_2 molecules only), sampled over the whole trajectories.

simulations of a single unit cell of S1L4 hydrogen hydrate (504 atoms) with ML on and ML off. For the simulations performed in this work, ML on provided a speedup of 1-3 orders of magnitude, depending on the length of the simulation. A few simple benchmark properties were used to compare the two, including temperature, pressure, potential energy, H_2 mean squared displacement (MSD), oxygen-oxygen RDF and hydrogen-hydrogen RDF (considering only H atoms of H_2). The results, shown in Fig. 3, reveal that both methods generated closely resembling simulation trajectories with no significant discrepancies. System properties, including energy, pressure, and temperature show the same mean and variance in the two trajectories.

The monitored RDFs of water oxygen atoms and hydrogen gas molecules are indistinguishable. Finally, the H₂ MSD is nearly identical in the two trajectories. Any minor differences are attributed to the chaotic nature of molecular dynamics, causing simulation trajectories to diverge over time due to differences in randomness between ML-AIMD and AIMD (similar to independent simulation trajectories using the same method with different random seed). Longer simulations using ML-AIMD are well-behaved, as was demonstrated in Fig. 1b, showing no signs of “blowing up” or drifting towards nonphysical behaviour. Finally, the velocity auto-correlation functions of the ML-AIMD and AIMD simulations were evaluated. Both methods had nearly identical velocity auto-correlation function, with no visible trends and negligible values (~ 0.01) after 0.25 ps, indicating that these 2.5 ps simulation trajectories are well equilibrated. The additional error introduced by ML-AIMD appears insignificant compared to the inherent inaccuracies of AIMD or the empirical models in FFMD. These results indicate that ML-AIMD is suitable for the present hydrogen hydrate system, providing reliable ab-initio reference data to be compared with FFMD in model verification. Nevertheless, as with most simulation methods, caution should be exercised to ensure physically significant results, and ML-AIMD should be more comprehensively tested for larger-scale use depending on the specific studies.

References

- [1] M. J. Abraham, T. Murtola, R. Schulz, S. Páll, J. C. Smith, B. Hess, and E. Lindahl, “Gromacs: High performance molecular simulations through multi-level parallelism from laptops to supercomputers,” *SoftwareX*, vol. 1–2, p. 19–25, Sept. 2015.
- [2] G. Kresse and J. Hafner, “Ab initio molecular dynamics for liquid metals,” *Physical Review B*, vol. 47, p. 558–561, Jan. 1993.
- [3] G. Kresse and J. Furthmüller, “Efficiency of ab-initio total energy calculations for metals

- and semiconductors using a plane-wave basis set,” *Computational Materials Science*, vol. 6, p. 15–50, July 1996.
- [4] G. Kresse and J. Furthmüller, “Efficient iterative schemes for ab initio total-energy calculations using a plane-wave basis set,” *Physical Review B*, vol. 54, p. 11169–11186, Oct. 1996.
- [5] G. Kresse and D. Joubert, “From ultrasoft pseudopotentials to the projector augmented-wave method,” *Physical Review B*, vol. 59, p. 1758–1775, Jan. 1999.
- [6] L. Landau, “Statistical physics,” 1969.
- [7] R. Jinnouchi, J. Lahnsteiner, F. Karsai, G. Kresse, and M. Bokdam, “Phase transitions of hybrid perovskites simulated by machine-learning force fields trained on the fly with bayesian inference,” *Phys. Rev. Lett.*, vol. 122, p. 225701, Jun 2019.
- [8] R. Jinnouchi, F. Karsai, and G. Kresse, “On-the-fly machine learning force field generation: Application to melting points,” *Phys. Rev. B*, vol. 100, p. 014105, Jul 2019.
- [9] R. Jinnouchi, F. Karsai, C. Verdi, R. Asahi, and G. Kresse, “Descriptors representing two- and three-body atomic distributions and their effects on the accuracy of machine-learned inter-atomic potentials,” *The Journal of Chemical Physics*, vol. 152, p. 234102, 06 2020.